

# Interferometry Radii at RHIC BES Energies within the integrated HydroKinetic Model

Vladislav Naboka,<sup>1,\*</sup> Yuri Sinyukov,<sup>1,2,†</sup> Musfer Adzhymambetov,<sup>1</sup> and Hanna Zbroszczyk<sup>2</sup>

<sup>1</sup>*Bogolyubov Institute for Theoretical Physics, Metrolohichna 14b, 03143 Kyiv, Ukraine*

<sup>2</sup>*Warsaw University of Technology, Faculty of Physics, Koszykowa 75, 00-662 Warsaw, Poland*

(Dated: June 25, 2025)

This study presents a correlation femtoscopy analysis of relativistic heavy-ion collisions at RHIC Beam Energy Scan (BES) energies using the extended integrated HydroKinetic Model (iHKMe). The model combines initial conditions from UrQMD transport simulations, a gradual pre-equilibrium relaxation stage, viscous hydrodynamic evolution, and a hadronic cascade, providing a comprehensive description of the system's full dynamical evolution. Special emphasis is placed on the impact of extended nuclear overlap times and partial thermalization, which are characteristic of intermediate collision energies ( $\sqrt{s_{NN}} = 7.7\text{--}39$  GeV).

The corresponding correlation femtoscopy scales, or interferometry (HBT) radii, are calculated across a range of collision energies and compared with experimental data to assess the sensitivity of femtoscopy observables to the equation of state (EoS). Two EoS scenarios are explored. The model demonstrates good agreement with experimental femtoscopy measurements, particularly at lower BES energies. These results enhance our understanding of the space-time structure of the particle-emitting source and provide valuable insight into the nature of the QCD phase transition in the intermediate energy regime.

## I. INTRODUCTION

Relativistic heavy-ion collisions have long served as a powerful tool for exploring the properties of strongly interacting matter under extreme conditions of temperature, baryon density, and energy density. Such conditions, achieved at facilities like the Relativistic Heavy Ion Collider (RHIC) and the Large Hadron Collider (LHC), are believed to resemble those that existed in the early Universe, microseconds after the Big Bang [1]. A central objective of these experiments is to study the formation and evolution of the quark-gluon plasma (QGP) and to investigate the nature of the transition between deconfined and confined phases of quantum chromodynamics (QCD) matter [2, 3].

In recent years, experimental programs have increasingly turned their attention to lower collision energies—particularly through the RHIC Beam Energy Scan (BES) program—where it has become evident that the underlying physical conditions differ significantly from those at top RHIC or LHC energies [4]. At lower center-of-mass energies ( $\sqrt{s_{NN}}$ ), the nuclear overlap time ( $\tau_{\text{overlap}} \approx 1\text{--}4$  fm/c) is no longer negligible compared to the prethermalization timescale, net baryon densities are substantial, and full thermalization may not be achieved. Moreover, the phase transition between hadronic and partonic matter is expected to exhibit critical

behavior, potentially indicating the presence of a critical endpoint in the QCD phase diagram [5, 6].

A key method for probing the space-time structure of the particle-emitting source is two-particle interferometry [7, 8], commonly referred now as correlation femtoscopy or sometimes (not quite correctly, see below) as Hanbury Brown–Twiss (HBT) [9] analysis. Measurements of identical particle correlations enable the extraction of interferometry radii, which are sensitive to both the geometric size and dynamic evolution of the system. Accurately modeling these observables requires a realistic description of the full system evolution, including pre-equilibrium dynamics, thermalization, hydrodynamic expansion, and freeze-out processes.

Several studies have utilized correlation to investigate the space-time structure of particle emission in heavy-ion collisions [10–14]. In the EPOS-based study [10], femtoscopy pion correlations were simulated for Au+Au collisions at BES energies, and the extracted HBT radii were compared to experimental data. THERMINATOR-based studies provide a statistical framework, replicating pion correlation patterns across varying collision energies [11]. In the work by Li et al. [12] HBT radii were researched for lower energies  $\sqrt{s_{NN}} = 2.4\text{--}7.7$  GeV. It emphasizes the sensitivity of HBT radii, particularly  $R_O/R_S$  and  $R_O^2 - R_S^2$ , to the equation of state (EoS), revealing signatures of phase transitions in the QCD matter. These models, both microscopic and macroscopic, highlight differing emission durations and source sizes as possible indicators of

\* [nvlad1@ukr.net](mailto:nvlad1@ukr.net)

† [Yu.Sinyukov@gmail.com](mailto:Yu.Sinyukov@gmail.com)

the QGP phase and critical point. Comparative analyses between cascade and hybrid models further stress the importance of EoS stiffness.

The integrated HydroKinetic Model (iHKM) [15–17] was developed to simulate the entire evolution of ultrarelativistic nuclear collisions and has successfully reproduced a wide range of observables at top RHIC and LHC energies. It incorporates all major stages of the collision process: initial state generation, pre-equilibrium relaxation, viscous hydrodynamic evolution, particlization, and a subsequent hadronic cascade. Previous studies have shown that iHKM provides a robust description of particle spectra, flow coefficients, and femtoscopic radii at high energies [18].

To address the challenges associated with modeling collisions at lower beam energies, a recently *extended* version of iHKM (iHKMe) has been developed [19]. In this work, we apply the updated framework to collisions in the GeV energy range, where the system experiences longer nuclear overlap times, slower thermalization, and possibly incomplete QGP formation. Unlike the original formulation [15], the extended model incorporates the effects of high net baryon density into both the equation of state and the dynamical evolution of conserved charge currents. Additionally, it features a smooth transition from the initial non-equilibrium phase, modeled via UrQMD transport dynamics [20, 21], to viscous hydrodynamics during the pre-equilibrium relaxation stage.

In our previous work [22], we calibrated the model parameters for RHIC BES energies based on heuristic arguments and transverse momentum spectra analyses. Two scenarios for the equation of state (EoS) of strongly interacting matter were considered: one assuming a smooth crossover transition [23], and the other featuring a first-order phase transition between hadronic matter and the QGP [24]. Interestingly, both EoS scenarios yielded comparably good agreement with the measured light hadron spectra. At higher BES energies (14.5 GeV and above), most model parameters required minimal adjustment, as the rapid system expansion reduces sensitivity to the details of the phase transition.

However, transverse momentum spectra alone provide limited information about the space-time characteristics of the particle-emitting source. Consequently, more sensitive observables are needed to further constrain the dynamics and probe the nature of the QCD phase transition. In this paper, we focus on the pion Bose–Einstein

correlations, that have also known as correlation femtoscopy or HBT analyses. The extracted interferometry radii reflect the system’s spatial and temporal evolution and are influenced by collective flow and expansion dynamics. We perform three-dimensional Gaussian fits to the correlation functions to extract these radii and assess their sensitivity to the underlying physics. We present results from three-dimensional fits to the correlation functions, assuming a Gaussian source shape characterized by the lengths of homogeneity:  $R_{\text{out}}$ ,  $R_{\text{side}}$ , and  $R_{\text{long}}$ .

The structure of this paper is as follows: In Sec. II, we provide a detailed description of the extended iHKM framework as adapted for RHIC BES energies. In Sec. III, we discuss the calibration of model parameters and present our results for interferometry radii. Finally, in Sec. IV, we summarize our findings and outline potential directions for future research.

## II. INTEGRATED HYDROKINETIC MODEL

### A. Model description

The integrated HydroKinetic Model (iHKM) was developed to simulate ultrarelativistic heavy-ion collisions [15]. It has successfully reproduced a broad range of observables, including hadron yields, transverse momentum spectra, flow coefficients, and interferometry radii [18, 25–31]. Recently, the model has been extended to lower collision energies [19], making it applicable to RHIC Beam Energy Scan (BES) and upcoming FAIR experiments.

This section briefly outlines the five stages of the iHKM framework: initial state generation, pre-equilibrium relaxation, viscous hydrodynamic evolution, particlization, and the subsequent hadronic cascade.

#### 1. Initial state generation

Accurate modeling of ultrarelativistic heavy-ion collisions begins with generating realistic initial conditions. At high collision energies, we use the Monte Carlo Glauber model [32]. At lower energies, however, the nuclear overlap time becomes comparable to the thermalization timescale—on the order of a few fm/c - necessitating a dynamical treatment of initial state formation.

To capture this early, non-equilibrium stage, we employ the Ultrarelativistic Quantum Molecular Dynamics (UrQMD) model [20, 21], a microscopic transport approach that describes

hadron and resonance interactions in detail. UrQMD simulates the nucleon-nucleon collisions and secondary interactions that create the hot and dense medium. We use the event-by-event UrQMD output to construct the energy-momentum tensor and baryon current, which serve as initial conditions for the subsequent hydrodynamic stage.

## 2. Relaxation stage

The matter produced in the early UrQMD evolution is far from equilibrium and requires thermalization before hydrodynamics can be applied. This motivates the introduction of a relaxation stage, during which the system evolves gradually toward local equilibrium. The approach is inspired by the relaxation-time approximation to the Boltzmann equation [16, 17]. The relaxation stage starts at a proper time  $\tau_0$  and lasts until the time  $\tau_{th}$ , both being the free parameters of the model. The total energy-momentum tensor and baryon charge current are taken in the form

$$T_{\text{total}}^{\mu\nu}(x) = T_{\text{urqmd}}^{\mu\nu} \cdot \mathcal{P}(\tau) + T_{\text{hydro}}^{\mu\nu} \cdot (1 - \mathcal{P}(\tau)), \quad (1)$$

thus, representing a sum of two components: a nonequilibrium component constructed from UrQMD and an equilibrium one (hydrodynamic tensors with viscous corrections). The weight function  $\mathcal{P}(\tau)$  should satisfy the following conditions:  $0 \leq \mathcal{P}(\tau) \leq 1$ ,  $\mathcal{P}(\tau_0) = 1$ ,  $\mathcal{P}(\tau_{th}) = 0$ ,  $\partial_\mu \mathcal{P}(\tau_{th}) = 0$ . The same can be written for the baryon current:

$$J_{\text{total}}^\mu(x) = J_{\text{urqmd}}^\mu \cdot \mathcal{P}(\tau) + J_{\text{hydro}}^\mu \cdot (1 - \mathcal{P}(\tau)), \quad (2)$$

For  $\mathcal{P}(\tau)$  we use the following ansatz:

$$\mathcal{P}(\tau) = \left( \frac{\tau_{th} - \tau}{\tau_{th} - \tau_0} \right)^{\frac{\tau_{th} - \tau_0}{\tau_{rel}}}, \quad (3)$$

where  $\tau_{rel}$  is another free parameter that defines the speed of the relaxation process.

## 3. Hydrodynamic stage

Once thermalization is achieved, the system evolves according to relativistic viscous hydrodynamics, governed by the conservation of energy-momentum and baryon number.

A key input is the equation of state (EoS), which relates energy density, pressure, and conserved charge densities (baryon number, electric charge, strangeness) to temperature and chemical potentials. The EoS characterizes both the

quark-gluon plasma and hadronic phases and incorporates either a smooth crossover or a first-order phase transition. Both cases are considered in this study.

While ideal hydrodynamics assumes vanishing viscosity, realistic modeling includes shear (and sometimes bulk) viscosity. In this work, only shear viscosity is considered, characterized by the ratio  $\eta/s$ .

When the medium becomes sufficiently dilute, the system transitions to the hadronic cascade via UrQMD, based on a fixed energy density criterion.

## 4. Particlization

The hydrodynamic evolution continues until the system departs from local equilibrium. At this point, we use the Cooper-Frye prescription [33] to convert the fluid into individual hadrons—a process known as particlization.

This transition occurs on a hypersurface of constant energy density  $\epsilon_{sw}$ , which is a model parameter and is fixed for each EoS scenario, independent of collision energy. The hypersurface is constructed using the Cornelius algorithm [34, 35].

The transition from hydrodynamics to the hadron cascade occurs on a hypersurface of constant energy density  $\epsilon_{sw}$ , which is a free parameter of the model. Although in this work  $\epsilon_{sw}$  depends only on the type of equation of state (EoS), it remains fixed and does not vary with collision energy. The particlization hypersurface is constructed during the hydrodynamic evolution using the Cornelius routine [34, 35].

When the particlization hypersurface  $\sigma^\mu$ , with all thermodynamic properties of the system on it, is defined, we apply the Cooper-Frye formula to convert the fluid into a cascade of particles:

$$p^0 \frac{d^3 N_i(x)}{d^3 p} = d\sigma_\mu p^\mu f_i(x, p), \quad (4)$$

Similarly to Eq. (1), the distribution function  $f_i(x, p)$  for particle species  $i$  consists of two components when the hypersurface  $\sigma$  enters the relaxation stage, i.e., for  $\tau < \tau_{th}$ . For the hypersurface with  $\tau \geq \tau_{th}$ , the distribution function takes the common form of the Bose (Fermi) equilibrium distribution with a small viscous correction. For further details, we refer the readers to [19].

## 5. Hadron gas cascade

The hadrons produced at particlization are fed into UrQMD for further evolution. Since

UrQMD operates on a constant-time hypersurface  $t=\text{const}$ , while our particlization surface is not, particles are propagated backward in time (without interactions) to align with UrQMD input requirements. The subsequent evolution, including rescattering and decay, proceeds until  $t=400\text{fm}/c$ , beyond which kinetic freeze-out is assumed. Particle positions and momenta at this stage are used to compute observables such as interferometry radii.

### B. Parameters of the model

To achieve our goals of describing the HBT-radii at different collision energies, we consider different values of collision energy  $\sqrt{s_{NN}}$ : 7.7, 11.5, 14.5, 19.6, 27, and 39 GeV. For the lower three energies, we also consider two different equations of state (EoS):

1. The equation of state that implies a crossover transition from QGP to hadron gas (CO, Chiral EoS)
2. The equation of state that implies a first-order phase transition (PT, phase transition EoS)

Thus, by comparing the results obtained using different EoS for the same collision energy, we can conclude which transition type leads to a better description of observables: crossover or first-order phase transition. For higher energies, we consider only the Chiral (crossover) EoS. In our model, we have the following free parameters mentioned in the previous section:

- $R$  [fm] – Gaussian smearing parameter used for making UrQMD initial conditions smoother for the relaxation stage.
- $\tau_0$  [fm/c] – the starting time of the relaxation stage
- $\tau_{\text{rel}}$  [fm/c] – relaxation time, which defines the speed of relaxation process
- $\tau_{\text{th}}$  [fm/c] – the finishing time of the relaxation stage and, subsequently, the start of the pure hydrodynamic stage
- $\eta/s$  – shear viscosity to entropy density ratio
- $\epsilon_{\text{sw}}$  [GeV/fm<sup>3</sup>] – energy density corresponding to the transition from the hydrodynamic stage to the hadron gas stage

For the sake of simplicity, we consider only the maximum possible value for the relaxation time:

$$\tau_{\text{rel}} = \tau_{\text{th}} - \tau_0. \quad (5)$$

In this paper, we use our previous results for the model parameter values [22]. Their values are presented in Table I.

Table I. Parameters of iHKM used for the calculation of interferometry radii.

$\sqrt{s_{NN}}$	EoS	R	$\tau_0$	$\tau_{th}$	$\eta / s$	$\epsilon_{sw}$
7.7	PT	0.5	2.6	3.2	0.08	0.35
7.7	CO	0.5	2.6	3.6	0.14	0.50
11.5	PT	0.5	2.0	2.6	0.08	0.35
11.5	CO	0.5	1.8	3.2	0.14	0.50
14.5	PT	0.5	1.4	2.0	0.08	0.35
14.5	CO	0.5	1.4	2.0	0.14	0.50
19.6	CO	0.5	1.0	2.0	0.14	0.50
27.0	CO	0.5	0.8	1.8	0.14	0.50
39.0	CO	0.5	0.6	1.4	0.14	0.50

### C. Interferometry radii

The method of stellar intensity interferometry of Hanbury-Brown and Twiss was proposed in the late 1950s by astronomers Hanbury-Brown and Twiss for measuring the angular size of stars.[9] Later, in 70-es it was successfully transformed into the two-particle correlation femtoscopy/interferometry analysis of the homogeneity lengths in the matter formed in nuclear (or particle) collisions [8, 36]. The similarity and principal difference between HBT and correlation femtoscopy methods one can read in detail in [37]. The correlation femtoscopy/interferometry is a useful tool for studying the space-time structure of the particle-emitting source, see, for example, [38–40].

Interferometry radii should be considered more as homogeneity regions than the real geometric sizes of the emitting source.[41, 42] Mathematically, they are obtained from the two-particle momentum correlation function:

$$C(\vec{p}_1, \vec{p}_2) = \frac{E_1 E_2 dN / (d^3 \vec{p}_1 d^3 \vec{p}_2)}{(E_1 dN / (d^3 \vec{p}_1))(E_2 dN / (d^3 \vec{p}_2))} \quad (6)$$

After some transformations, it can be written in terms of the emission function  $S(x, p)$  [39]

$$C(\vec{q}, \vec{p}) = 1 \pm \frac{|\int d^4 x S(x, p) e^{iqx}|^2}{\int d^4 x S(x, p + \frac{1}{2}q) \int d^4 y S(y, p - \frac{1}{2}q)}. \quad (7)$$

where pair relative momenta  $q = p_1 - p_2$ , pair average momenta  $p = \frac{p_1 + p_2}{2}$ . Then, applying mass shell and smoothness approximation [39], this transforms to

$$C(\vec{q}, \vec{p}) \approx 1 \pm \left| \frac{\int d^4 x S(x, p) e^{iqx}}{\int d^4 x S(x, p)} \right|^2 = 1 \pm |\langle e^{iqx}(p) \rangle| \quad (8)$$

In the UrQMD event generator, this equation has the form

$$C(\vec{q}) = \frac{\sum_{i \neq j} \delta_{\Delta}(\vec{q} - \vec{p}_i + \vec{p}_j)(1 + \cos(\vec{p}_j - \vec{p}_i)(\vec{x}_j - \vec{x}_i))}{\sum_{i \neq j} \delta_{\Delta}(\vec{q} - \vec{p}_i + \vec{p}_j)}, \quad (9)$$

$\delta_{\Delta}(\vec{x}) = 1$  if  $|\vec{x}| < \Delta\vec{p}/2$  and 0 otherwise, where  $\Delta\vec{p}$  is the size of the bin in histogram. The correlation function histograms in this form for different pair relative momenta  $\vec{q}$  in the LCMS system are fitted with Gaussians for each  $\vec{p}$ :

$$C(\vec{q}) = 1 + \lambda \exp\left(-R_{out}^2 q_{out}^2 - R_{side}^2 q_{side}^2 - R_{long}^2 q_{long}^2\right) \quad (10)$$

The interferometry radii  $R_{out}(p_T)$ ,  $R_{side}(p_T)$ ,  $R_{long}(p_T)$  and the suppression parameter  $\lambda$  are extracted from this fit. In this work, we calculate the dependence of interferometry radii on transverse mass  $m_T = \sqrt{m^2 + p_T^2}$  to compare it with experimental data [43].

### III. RESULTS

For each parameter set, we perform 150 hydrodynamic simulations. From each simulation, we sample 200 UrQMD afterburner events, resulting in a total of 30,000 events per parameter set. All calculations in this study are carried out for the 5% most central collisions. Centrality is defined based on the multiplicity of charged particles. However, due to the limited number of hydrodynamic simulations, it is not feasible to define centrality classes with sufficient statistical precision directly from hydrodynamic data. Therefore, for each collision energy, we first generate 20,000 standalone UrQMD events, evolved up to 200 fm/c, to define centrality classes. We then select the top 5% most central events as initial conditions for the iHKM pre-equilibrium stage and the subsequent hydrodynamic evolution. In order to have enough statistics for pion pairs of close momentum, a batch of events is taken to calculate the two-particle correlation function.

The resulting HBT radii for lower collision energies ( $\sqrt{s_{NN}} = 7.7 - 14.5$  GeV) using the Chiral (crossover) EoS are presented in Fig. 1, while the corresponding results for the first-order phase transition EoS are shown in Fig. 2. As experimental data for 14.5 GeV are unavailable, we compare our results with data at neighboring energies, 11.5 and 19.6 GeV, under the assumption that the interferometry radii vary smoothly with collision energy. From these figures, we observe that the Chiral EoS provides a slightly better overall description of the HBT radii than the first-order

phase transition EoS. However, the performance of the first-order EoS improves as the collision energy decreases. This trend suggests that at even lower energies, such as 2–4 GeV, the first-order phase transition EoS may yield a more accurate description than the Chiral EoS.

As in the STAR data, our results for the *long* HBT radii show an increasing trend with collision energy. This behavior is commonly attributed to an extended system lifetime at higher energies, driven by the increased initial energy density [41]. In contrast, the experimental *side* and *out* HBT radii exhibit minimal dependence on collision energy. Although our model predicts slightly varying—but closely matching—values for these radii, it reproduces their overall energy independence.

At higher collision energies, we employ only the chiral EoS, as the first-order phase transition EoS fails to provide a satisfactory description of the interferometry radii. This is consistent with the expectation that a phase transition is unlikely to occur at high energies. The results for the chiral EoS in this regime are presented in Fig. 3. The model generally reproduces the trends observed in the experimental data. However, it noticeably overestimates the increase of the *long* radii with energy compared to the experimental results.

### IV. SUMMARY

In this work, we applied the recently extended integrated HydroKinetic Model to describe femtosopic observables in relativistic nucleus–nucleus collisions at the intermediate energies of the RHIC Beam Energy Scan program. The updated model accounts for essential features of lower-energy collisions, including significant baryon stopping, prolonged nuclear overlap times, and the possible partial thermalization of matter. Two scenarios for the equation of state of strongly interacting matter—a smooth crossover and a first-order phase transition—were investigated. The calculated femtosopic observables, particularly the interferometry radii over the broad energy range from 7.7 to 39 GeV, demonstrate the model’s capability to reproduce key experimental trends and offer insights into the QCD phase structure at intermediate energies.

Comparison with experimental data demonstrates that the extended iHKM framework provides a satisfactory description of the space-time structure of the particle-emitting source across the entire energy range. The results show that the interferometry radii are sensitive to the choice of EoS, offering potential insights into the nature of the QCD phase transition at intermediate collision energies.

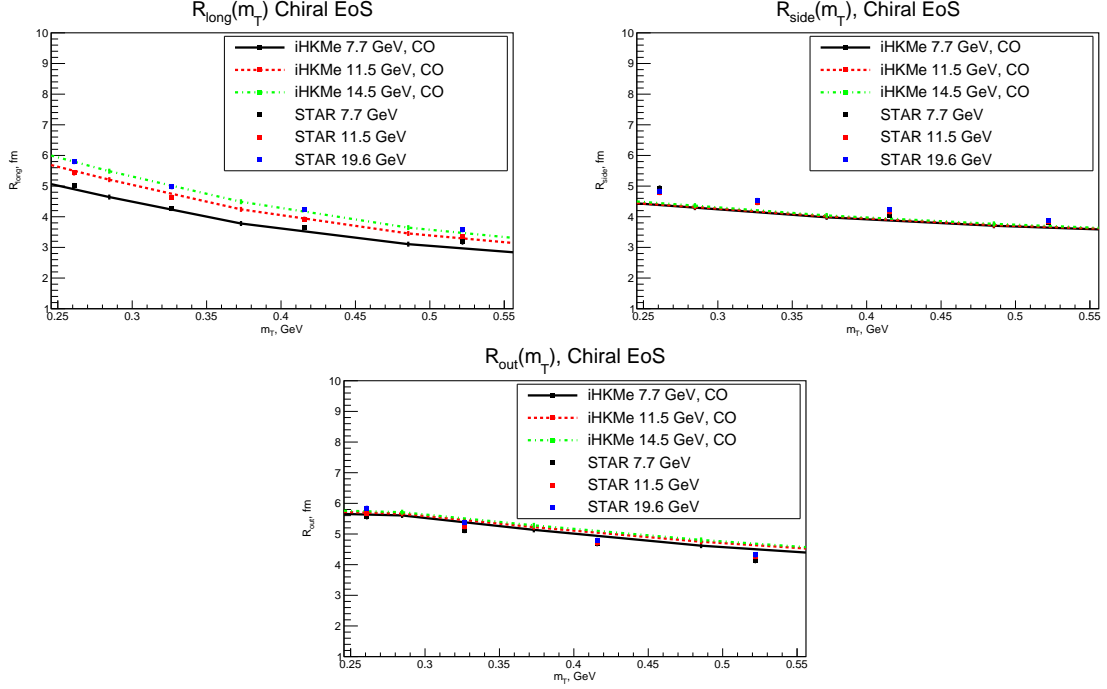


Figure 1. Results of calculations for  $R_{long}$ ,  $R_{side}$  and  $R_{out}$  for  $\pi^-$  pairs of 5% most central collisions of Au+Au at energies 7.7, 11.5 and 14.5 GeV. In these calculations, Chiral (crossover) EoS is used. The experimental data are taken from [43].

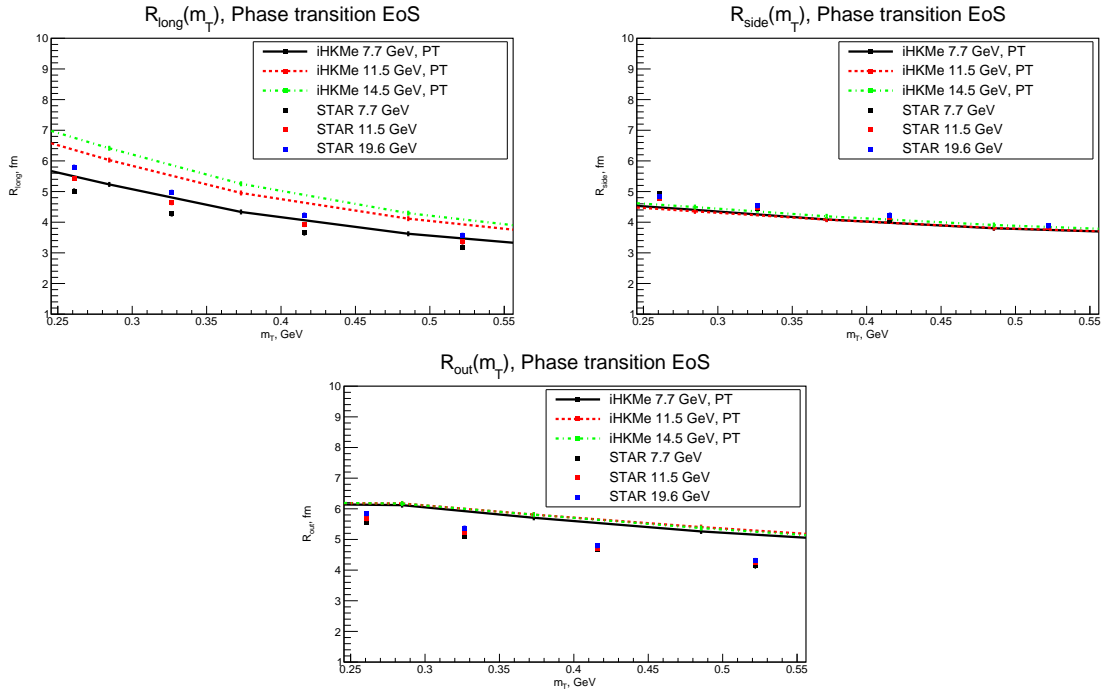


Figure 2. Results of calculations for  $R_{long}$ ,  $R_{side}$  and  $R_{out}$  for  $\pi^-$  pairs of 5% most central collisions of Au+Au at energies 7.7, 11.5 and 14.5 GeV. In these calculations, the first-order phase transition EoS is used. The experimental data is taken from [43].

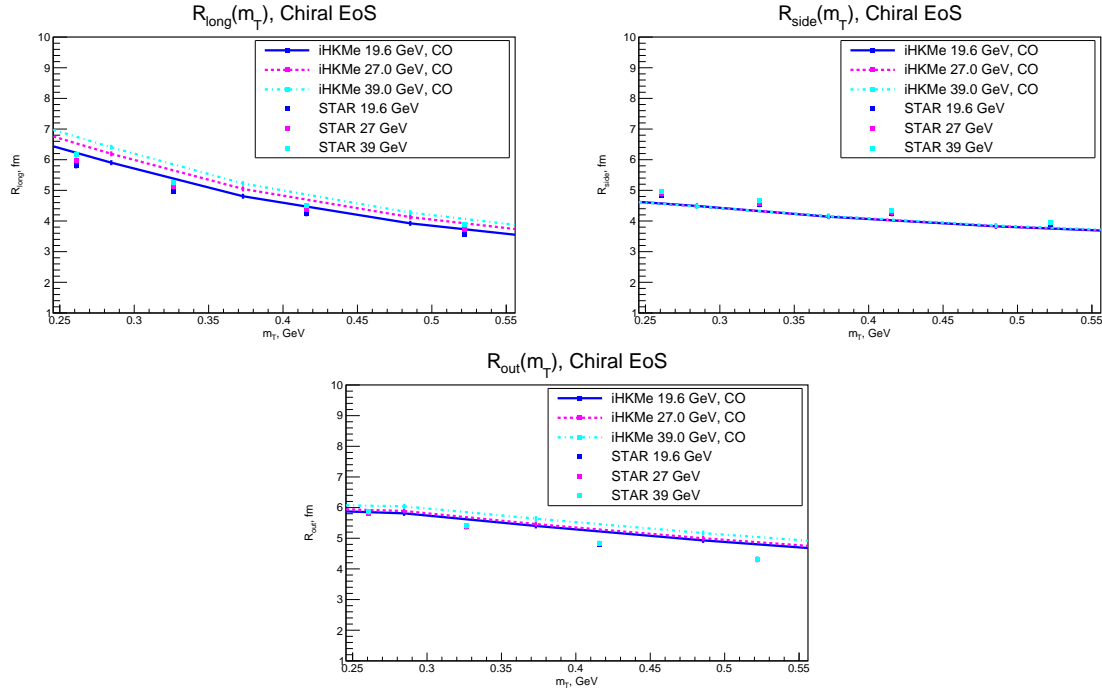


Figure 3. Results of calculations for  $R_{long}$ ,  $R_{side}$  and  $R_{out}$  for  $\pi^-$  pairs of 5% most central collisions of Au+Au at energies 19.6, 27 and 39 GeV. In these calculations, Chiral (crossover) EoS is used. The experimental data are taken from [43].

We find that the crossover EoS yields a better description of the interferometry radii, especially at higher BES energies, while at lower energies, such as 7.7 GeV, the first-order phase transition EoS also provides a reasonable agreement with the data. The *side* and *out* radii show minimal dependence on collision energy, whereas the *long* radius exhibits a clear increasing trend with energy.

Further refinements of the model and systematic studies are planned to deepen our understanding of the properties of strongly interacting

matter created in these collisions.

## ACKNOWLEDGMENTS

H.Z.'s work was supported by the Grant of National Science Centre, Poland, No: 2021/41/B/ST2/02409 and 2020/38/E/ST2/00019. The research of Yu. S. was partially funded by IDUB-POB projects granted by WUT (Excellence Initiative: Research University (ID-UB)). M.A. and V. N. gratefully acknowledge support from the Simons Foundation (Grant SFI-PD-Ukraine-00014578).

- 
- [1] J. Rafelski, Connecting qgp-heavy ion physics to the early universe, *Nuclear Physics B - Proceedings Supplements* **243-244**, 155 (2013), [arXiv:1306.2471 \[astro-ph.CO\]](#).
- [2] J. Adams *et al.* (STAR Collaboration), Experimental and theoretical challenges in the search for the quark gluon plasma: The star collaboration's critical assessment of the evidence from rhic collisions, *Nuclear Physics A* **757**, 102 (2005), [arXiv:nucl-ex/0501009](#).
- [3] K. Adcox *et al.* (PHENIX Collaboration), Formation of dense partonic matter in relativistic nucleus-nucleus collisions at rhic: Experimental evaluation by the phenix collaboration, *Nuclear Physics A* **757**, 184 (2005), [arXiv:nucl-ex/0410003](#).
- [4] G. Odyniec, The RHIC Beam Energy Scan program in STAR and what's next ..., in *Journal of Physics: Conference Series*, Vol. 455 (2013) p. 012037.
- [5] M. A. Stephanov, K. Rajagopal, and E. V. Shuryak, Signatures of the tricritical point in QCD, *Physical Review Letters* **81**, 4816 (1998), [arXiv:hep-ph/9806219](#).
- [6] M. A. Stephanov, K. Rajagopal, and E. V. Shuryak, Event-by-event fluctuations in heavy ion collisions and the qcd critical point, *Physical Review D* **60**, 114028 (1999), [arXiv:hep-](#)

- ph/9903292.
- [7] G. Goldhaber, S. Goldhaber, W. Lee, and A. Pais, Influence of bose-einstein statistics on the antiproton-proton annihilation process, *Physical Review* **120**, 300 (1960).
- [8] G. I. Kopylov, Like particle correlations as a tool to study the multiple production mechanism, *Physics Letters B* **50**, 472 (1974).
- [9] R. Hanbury-Brown and R. Q. Twiss, A test of a new type of stellar interferometer on sirius, *Nature* **178**, 1046 (1956).
- [10] M. Stefaniak and H. Zbroszczyk, Examination of the heavy-ion collisions using EPOS model in the frame of BES program at RHIC, *EPJ Web Conf.* **164**, 07013 (2017).
- [11] K. Brzeziński, P. Szymański, and H. Zbroszczyk, Two-particle correlations using THERMINATOR model for BES program, in *Acta Phys. Polon. B Proc. Suppl.*, Vol. 9 (2016) pp. 193–194.
- [12] P. Li, J. Steinheimer, T. Reichert, A. Kittiratpattana, M. Bleicher, and Q. Li, Effects of a phase transition on two-pion interferometry in heavy ion collisions at  $\sqrt{s_{NN}} = 2.4\text{--}7.7$  GeV, *Sci. China Phys. Mech. Astron.* **66**, 232011 (2023).
- [13] C. Zhang and J. Xu, Effects of hadronic mean-field potentials on Hanbury–Brown–Twiss correlations in relativistic heavy-ion collisions, *Phys. Rev. C* **96**, 044907 (2017), arXiv:1707.07272 [nucl-th].
- [14] P. Batyuk, D. Blaschke, M. Bleicher, Y. B. Ivanov, I. Karpenko, L. Malinina, S. Merts, M. Nahrgang, H. Elfner, and O. Rogachevsky, Three-fluid hydrodynamics-based event simulator extended by UrQMD final state interactions (THESEUS) for FAIR-NICA-SPS-BES/RHIC energies, in *Proceedings, 6th International Conference on New Frontiers in Physics (ICNFP 2017)*, EPJ Web Conf., Vol. 182 (2018) p. 02056, 1711.07959.
- [15] V. Y. Naboka, I. A. Karpenko, and Y. M. Sinyukov, Thermalization, evolution, and observables at energies available at the CERN Large Hadron Collider in an integrated hydrokinetic model of A+A collisions, *Phys. Rev. C* **93**, 024902 (2016), arXiv:1508.07204 [hep-ph].
- [16] S. V. Akkelin and Y. M. Sinyukov, Matching of nonthermal initial conditions and hydrodynamic stage in ultrarelativistic heavy-ion collisions, *Phys. Rev. C* **81**, 064901 (2010), arXiv:0912.4180 [nucl-th].
- [17] V. Y. Naboka, S. V. Akkelin, I. A. Karpenko, and Y. M. Sinyukov, Initialization of hydrodynamics in relativistic heavy ion collisions with an energy-momentum transport model, *Phys. Rev. C* **91**, 014906 (2015), arXiv:1411.4490 [nucl-th].
- [18] V. M. Shapoval, M. D. Adzhymambetov, and Y. M. Sinyukov, Femtoscopy scales and particle production in the relativistic heavy ion collisions from Au+Au at 200 AGeV to Xe+Xe at 5.44 ATeV within the integrated hydrokinetic model, *Eur. Phys. J. A* **56**, 260 (2020), arXiv:2006.16697 [nucl-th].
- [19] M. Adzhymambetov and Y. Sinyukov, Extension of the integrated HydroKinetic Model to BES RHIC and GSI-FAIR nuclear collision energies (2024), arXiv:2412.00458 [hep-ph].
- [20] S. A. B. et al., Microscopic models for ultrarelativistic heavy ion collisions, *Progress in Particle and Nuclear Physics* **41**, 255 (1998), arXiv:nucl-th/9803035 [nucl-th].
- [21] M. B. et al., *Journal of Physics G* **25**, 1859 (1999), arXiv:hep-ph/9909407 [hep-ph].
- [22] N. Rathod, Y. Sinyukov, M. Adzhymambetov, and H. Zbroszczyk, Particle Spectra in the Integrated HydroKinetic Model at RHIC BES Energies (2025), arXiv:2506.13944 [nucl-th].
- [23] J. Steinheimer, S. Schramm, and H. Stocker, An Effective chiral Hadron-Quark Equation of State, *J. Phys. G* **38**, 035001 (2011), arXiv:1009.5239 [hep-ph].
- [24] P. F. Kolb and U. W. Heinz, Hydrodynamic description of ultrarelativistic heavy ion collisions, Part of Quark-gluon plasma 4 (2003), arXiv:nucl-th/0305084.
- [25] Y. Sinyukov, V. Shapoval, and V. Naboka, On mT dependence of femtoscopy scales for meson and baryon pairs, *Nuclear Physics A* **946**, 227 (2016), arXiv:1508.01812 [hep-ph].
- [26] V. Shapoval, Y. Sinyukov, and V. Naboka, Proton-lambda correlation functions at energies available at the CERN Large Hadron Collider taking into account residual correlations, *Phys. Rev. C* **92**, 044910 (2015), arXiv:1509.04245 [hep-ph].
- [27] V. Naboka, Y. Sinyukov, and G. Zinovjev, Direct-photon spectrum and elliptic flow produced from Pb+Pb collisions at energy 2.76 TeV at the CERN Large Hadron Collider within an integrated hydrokinetic model, *Phys. Rev. C* **97**, 054907 (2018), arXiv:1710.07689 [hep-ph].
- [28] V. Naboka, Y. Sinyukov, and G. Zinovjev, Photon spectra and anisotropic flow in heavy ion collisions at the top RHIC energy within the integrated hydrokinetic model with photon hadronization emission, *Nuclear Physics A* **1000**, 121843 (2020), arXiv:1912.01423 [nucl-th].
- [29] Y. M. Sinyukov, M. D. Adzhymambetov, V. Y. Naboka, and V. M. Shapoval, The prethermal stage of heavy-ion collision and the particle production, *Acta Physica Polonica B, Proceedings Supplement* **11**, 633 (2018).
- [30] M. D. Adzhymambetov, V. Y. Naboka, V. M. Shapoval, and Y. M. Sinyukov, The femtoscopy scales in Au+Au collisions at the top RHIC energy, *Acta Physica Polonica B Proceedings Supplement* **12**, 10.5506/APhysPolB-Supp.12.235 (2019).
- [31] Y. M. Sinyukov, M. D. Adzhymambetov, V. M. Shapoval, and V. Y. Naboka, Femtoscopic structure of relativistic heavy ion collisions in the integrated hydrokinetic model, *Physics of Particles and Nuclei* **51**, 258 (2020).
- [32] M. Alvioli, H.-J. Drescher, and M. Strikman, A monte carlo generator of nucleon configurations in complex nuclei including nucleon-nucleon correlations, *Physics Letters B* **680**, 225 (2009).
- [33] F. Cooper and G. Frye, Comment on the single particle distribution in the hydrodynamic

- and statistical thermodynamic models of multi-particle production, *Physical Review D* **10**, 186 (1974).
- [34] P. Huovinen and H. Petersen, Particlization in hybrid models, *European Physical Journal A* **48**, 171 (2012), [arXiv:1206.3371 \[nucl-th\]](#).
- [35] S. Pratt, Accounting for backflow in hydrodynamic-boltzmann interfaces, *Physical Review C* **89**, 024910 (2014).
- [36] A. N. Makhlin and Y. M. Sinyukov, Hadron matter under pion interferometry microscope, *Zeitschrift für Physik C* **39**, 69 (1988).
- [37] Y. M. Sinyukov and V. M. Shapoval, Correlation femtoscopy of small systems, *Physical Review D* **87**, 094024 (2013).
- [38] U. Heinz, Hanbury-brown/twiss interferometry for relativistic heavy-ion collisions: Theoretical aspects (1997), lectures at NATO ASI "Correlations and Clustering Phenomena in Subatomic Physics", Dronten, Aug 4-18, 1996, [arXiv:nucl-th/9609029 \[nucl-th\]](#).
- [39] U. Heinz and B. V. Jacak, Two-Particle Correlations in Relativistic Heavy-Ion Collisions, *Ann.Rev.Nucl.Part.Sci* **49**, 529 (1999), [arXiv:nucl-th/9902020 \[nucl-th\]](#).
- [40] U. A. Wiedemann and U. Heinz, Particle interferometry for relativistic heavy-ion collisions, *Physics Reports* **319**, 145 (1999), [nucl-th/9901094](#).
- [41] S. V. Akkelin and Y. M. Sinyukov, The HBT-interferometry of expanding inhomogeneous sources, *Z. Phys. C* **72**, 501 (1996).
- [42] Y. M. Sinyukov, S. V. Akkelin, and A. Y. Tolstykh, Interferometry radii for expanding hadron resonance gas, *Nuclear Physics A* **610**, 278 (1996).
- [43] L. A. et al. (STAR), Beam-energy-dependent two-pion interferometry and the freeze-out eccentricity of pions measured in heavy ion collisions at the STAR detector, *Phys. Rev. C* **92**, 014904 (2015), [arXiv:1403.4972v1 \[nucl-ex\]](#).